Research on Engineering Structures & Materials
www.jresm.org
Research Group

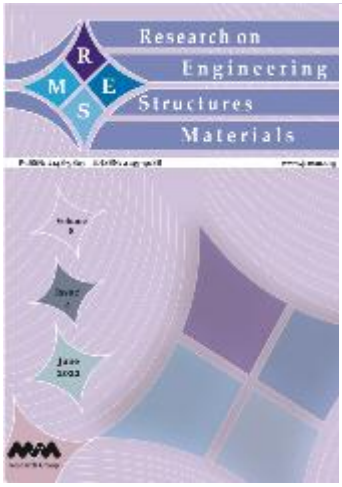


# Friction stir-welding of AZ31B Mg and 6061-T6 Al alloys optimization using Box-Behnken design (BBD) and Artificial Neural network (ANN)

Dame Alemayehu Efa, Endalkachew Mosisa Gutema, Hirpa G. Lemu, Mahesh Gopal

Online Publication Date: 20 October 2023
URL: http://www.jresm.org/archive/resm2023.50ma0703rs.html
DOI: http://dx.doi.org/10.17515/resm2023.50ma0703rs
Journal Abbreviation: *Res. Eng. Struct. Mater.*

**To cite this article**
Efa DA, Gutema EM, Lemu HG, Gopal M. Friction stir-welding of AZ31B Mg and 6061-T6 Al alloys optimization using Box-Behnken design (BBD) and Artificial Neural network (ANN). *Res. Eng. Struct. Mater.*, 2024; 10(1): 413-430.

Research on Engineering Structures & Materials
www.jresm.org
Research Group

*Research Article*

# Friction stir-welding of AZ31B Mg and 6061-T6 Al alloys optimization using Box-Behnken design (BBD) and Artificial Neural network (ANN)

Dame Alemayehu Efa[1a], Endalkachew Mosisa Gutema*[1b], Hirpa G. Lemu[2c], Mahesh Gopal[1d]

[1]*Dept. of Mechanical Eng., College of Eng. and Technology, Wollega University, Nekemte, Ethiopia*
[2]*Dept. of Mechanical and Structural Eng. and Materials Science, Faculty of Science and Technology, University of Stavanger, N-4036 Stavanger, Norway*

**Article Info**

*Article history:*

Received 03 June 2023
Accepted 12 Oct 2023

*Keywords:*

*Box-Behnken design;*
*Response surface methodology;*
*Friction stir-welding;*
*COMSOL multiphysics® 6.0 software;*
*Artificial neural network;*
*Peak temperature*

**Abstract**

The primary goal of the study is to optimize the welding parameters using Friction Stir Welding (FSW) to join AZ31B Mg and AA 6061 alloys considering input parameters such as rotational speed, welding speed, shoulder-to-pin diameter ratio and plunge force and output parameters as peak temperature. The simulation experiment is carried out using COMSOL Multiphysics® 6.0 Software. The simulation experiment is designed using the Box-Behnken design (BBD) of Response Surface Methodology (RSM) and mathematical models were developed. The Analysis of Variance (ANOVA) is used to assess the features of the performance effectiveness of the parameters. Both direct and indirect interaction effects are investigated; the results indicate that the rotational speed is the most influential parameter when compared to other factors; as rotational speed increases consequently; there is an increase in temperature. Finally, the Artificial Neural Network was trained and tested in MATLAB software to optimize the parameters. The validation was performed to predict the minimal predicted temperature value. The confirmatory tests reveal that the predicted results are extremely close to the experimental values from the simulation.



## 1. Introduction

The joining of dissimilar metals is a challenge by the conventional joining process due to the physical, thermal, mechanical and chemical properties of different materials and also the welding of dissimilar metals at low melting temperatures, and high thermal conductivity, which are difficult to weld using conventional welding techniques. FSW is the solid-state joining technique in which the materials are joined without melting the workpiece. Heat is generated in the FSW process as a result of thermo-mechanical deformation and relative motion between the tool and workpiece. The material flow plasticized behind the tool as a result of the rotating tool's forward translation motion along the joint line under axial pressure and heat transfer at the plate's edge. The dissimilar metals like magnesium, aluminum, steel, copper and titanium are joined using the FSW process.

The simulation experiment using FEM techniques was conducted to study the thermal phenomenon during the welding of dissimilar metals of AZ31B-H24 Magnesium alloys and Aluminum 6061-T6 to predict peak temperature using the FSW process. The results indicate that peak temperature was more reliant on shoulder diameter and tool traverse speed than on tool rotation speed. The peak temperature is directly proportional to tool rotation speed and

*Corresponding author: endalkachewm@wollegauniversity.edu.et
[a] orcid.org/0009-0003-4112-7278; [b] orcid.org/0000-0002-1628-7216; [c] orcid.org/0000-0001-9588-4707; [d]orcid.org/0000-0001-7672-5399
DOI: http://dx.doi.org/10.17515/resm2023.50ma0703rs

shoulder diameter and inversely proportional to tool traverse speed [1]. The microstructure and mechanical characteristics of magnesium alloys to Aluminum alloy 6061-T6 of the FSW specimens were studied using elemental analysis. The elemental analysis of the AZ91D to 6061-T6 Al weld reveals that the Al and Mg distributions are more uniform in the FSW zone [2]. The research in (3) provides valuable insight into the welding and softening behavior of Al 6061-T6 and Mg AZ31B dissimilar alloys in FSW. It demonstrates that softening occurs throughout the FSW Al 6061-T6 alloy owing to the dissolving of the strengthening precipitates: In contrast, it occurs mostly within the stir zone due to localized textural differences in the FSW Mg AZ31B alloy.

The processing parameters on the microstructure and mechanical characteristics of FSW joints of AZ31B Magnesium alloy and 6061-T6 Aluminum alloy are examined by (4) concluded that the optimum joint quality is achieved at 1600 rpm of rotational speed and 500 mm/min of translational speed. AZ31B magnesium and Al6061-T6 Aluminum were used in the FSW process. Detailed microstructural research was done to determine the composition of the intermetallic phases generated in the stirring zone and their effect on micro hardness and overall mechanical properties of the weld [5]. The studies were carried out to examine the effects of tool rotational speeds on the microstructure, hardness, and tensile characteristics of 6061-T6 Aluminum and AZ31B magnesium alloys. The findings revealed that rotational speeds influence the parameters and tensile characteristics increased and subsequently declined as welding speed increased. The maximum tensile strength was 137 MPa at a welding speed of 60 mm/min [6]. The purpose of the study was to investigate the microstructural and corrosion behavior of FSW joints between a 6061 Al and AZ31 Mg with a zirconium interlayer. The Zr interlayer prevented the formation of Al-Mg intermetallic compounds due to its synergetic actions of chemical alteration and thermal resistance [7]. The influence of tool offset on the microstructure and characteristics of AA6061/AZ31B Aluminum alloys was investigated in FSW. The results revealed that increasing the tool offset had a substantial influence on the microstructure, mechanical characteristics, and micro-hardness, with the joint strength reaching a maximum of 107 MPA when the offset reached 1.5mm [8]. The FSW experiment was performed to weld AA 6061-T6 and AZ31B alloys, with the welding parameters. The results show that at 400 rpm to 700 rpm of tool rotation speed, the average micro hardness value in the nugget zone first increases then decreases, and the micro hardness value within the stir zone is greater than the base metal, with the highest value being equal to twice of the base metal [9]. FSW was utilized to join incompatible AA6061-T6 alloys to AZ31B-H24 alloys while taking into account process characteristics such as rotating speed, welding speed, tool plunge depth, and tool pin shape. The results demonstrate that the M7 joint has the maximum tensile strength of 88.2 MPa and the lowest of 18.95 MPa in the M3 weld [10]. The butt joint was designed to weld 5A06 Al and AZ31B Mg alloys with 20 mm thickness using FSW and concluded that the highest hardness was 289 HV on the IMC layer of the Mg side interface, and the nanoindentation tests revealed that the nano hardness of the $Al_{12}Mg_{17}$ layer and $Al_3Mg_2$ layer was 5.39 GPa and 4.18 GPa, respectively [11]. The experiment was carried out with dissimilar metals AA 6061 and Mg AZ31B. The author demonstrated that the FSW joint has much higher strength and concluded that the weld line offset from the center was responsible for the deposition of larger concentrations of magnesium, which minimizes the Inter Metallic compounds and so enables a higher tensile strength of 39MPa [12]. FSW is used to join Aluminum Al-6062 and magnesium AZ31B, using spindle speed and welding speed as process parameters. As stated by the author, the welded joint strength of the Aluminum-Magnesium joint is 110% more than that of the magnesium-magnesium joint at maximum UTS, spindle speed and welding speed of 100rpm and 50mm/min with magnesium on the advancing side [13]. The microstructural and mechanical properties of the Refill Friction Stir Spot Welding process were examined utilizing AZ31B/AA6061 dissimilar joint. The results revealed that joining metals yielded higher static shear strength and concluded that welds with a tool rotational speed of 1400 rpm have a maximum static shear strength of 3.6 KN and when the rotating speed of the tool exceeds 1400

rpm, the static shear strength of the joints decreases [14]. The author [15] discussed the development of medium-thick AA6061 Al/AZ31B Mg dissimilar alloys during submerged friction stir welding and concluded that the ultimate tensile strength of dissimilar metal of Aluminum alloy 6061 and magnesium AZ31B was increased to 171 MPa and the strength of magnesium-magnesium AZ31B is approximately 71.3%. The computational fluid dynamics-based simulation experiment was done by [16] to investigate the mixing process and material flow in the FSW of AA6061-T6 and AZ31B mg alloys. Based on the simulation results, the material mixing is unstable throughout the FSW process, resulting in a fluctuant component distribution along the longitudinal direction in the joint's stir zone. The study used a statistical design of trials to explore the impact of tool positioning factors on peak temperature in dissimilar friction stir welding of the Aluminum alloys AA6061-T6 and AA7075-T6. The findings demonstrated that the plunge depth, tilt angle, and tool offset all had a significant influence on the peak temperature and tool offset. The greatest process temperature was created at a tilt angle of 1.8 degrees, and it declined for values less and greater than this angle. Peak temperature values were lowest in samples with greater tilt angles [17].

The ANSYS FLUENT software was employed to model 3D material flow variations during FSW utilizing varied pin profiles to reduce simulation time and increase simulation result dependability [18]. The investigation process was carried out by [19] to study the impact of the traverse and rotational velocities of the noncontact shoulder tool of the friction stir joining (FSJ) process of polyamide 6 (PA6) polymer and suggests that the material velocity raised at higher rotational speed and lesser transverse velocity and in the stir zone. The author [20] investigated the influence of tensile, impact, corrosion testing, fracture, and statistical and cost analysis on dissimilar junctions built of AA6061, AZ31B, and AZ91D. The results show that AZ91 and AZ31B have the highest tensile strength, whereas AA6061 and AZ91 have the highest yield strength. The friction stir welding (FSW) procedure was used to weld dissimilar alloys of magnesium and steel in order to analyze the heat changes, material flow, and mechanical characteristics during the process. The author [21] concludes that increasing the number of shoulders increases the frictional generation of heat.

In summary, the preceding research investigation primarily considered the effect of process parameters such as tool rotational speed, welding speed, and shoulder-to-pin diameter ratio on temperature obtained during FSW using the combination of various metals. Furthermore, these investigations sought to comprehend and characterize intermetallic phases, the effects of process factors on microstructural features, the evaluation of joint strength, the simulation of material mixing during welding, and techniques to enhance tool position in FSW.

However, despite extensive literature review, there is limited research available considering rotational speed, welding speed, shoulder-to-pin diameter ratio and Plunge force to measure the peak temperature during FSW welding and no studies compare the joining of AZ31B and AA 6061 material using FEA using COMSOL Multiphysics® 6.0 Software. This study aims to address the gap by providing an in-depth investigation of the FSW process of both materials and makes a contribution to the discipline by filling in gaps in the literature. The simulation design was carried out using Response Surface Methodology (RSM) and optimization was done using an Artificial Neural Network (ANN) to analyze the parameters influencing the welding of dissimilar metals 6061-T6 Al alloys and AZ31B Mg alloys. Thus the experiment was carried out to overcome the above mentioned challenges and solve the critical issues for the industry professionals to shorten total manufacturing time.

## 2. Mathematical Model

In this FSW modeling the following assumptions are made by the authors:

- The frictional heat is generated at the interface of the workpiece/shoulder.

- The flow of heat stopped after the workspace melting temperature become equal to local temperatures.
- The tool pin thread can be neglected as the pin is cylindrical.

The complicated process of the FSW process becomes simpler while moving the tool in the coordinate system. The heat transfer control equation for the work piece in a moving coordinate system with a positive x-direction moving tool is given by the equation 1 [22].

$$\frac{\partial(\rho cT)}{\partial t} = \frac{\partial}{\partial_x}\left(\lambda_x \frac{\partial T}{\partial_x}\right) + \frac{\partial}{\partial_y}\left(\lambda_y \frac{\partial T}{\partial_y}\right) + \frac{\partial}{\partial_z}\left(\lambda_z \frac{\partial T}{\partial_z}\right) + W_v \frac{\partial}{\partial_x}(\rho C_p T) \tag{1}$$

Heat is considered at the interface of the pin/work piece and shoulder/work piece in this model. Heat is generated in the pin through material shearing, threaded surface friction and friction on the pin itself is illustrated in equation 2. [24], [22].

$$\begin{aligned} &Q_{pin} = \frac{2\mu K \pi r_p t_w r_p}{\sqrt{3(1+\mu^2)}} + 2\pi r_p t_w K\tau \frac{V_m}{\sqrt{3}} + \frac{4F_p \mu V_m}{\pi} \cos\theta \\ &\theta = 90^o\text{-}\lambda_T\text{-}\tan^{-1}(\mu),\ V_{rp} = \frac{\sin\theta}{\sin(18^o-\theta-\lambda)} v_p,\quad V_m = \frac{\sin\lambda}{\sin(18^o-\theta-\lambda)} v_p \text{ and, } V_p = r_p\omega \end{aligned} \tag{2}$$

The heat flux per unit area ($W/m^2$) function of distance r from the shoulder's center axis is defined as shown in equation 3. [1], [25].

$$q_s(r,T) = \begin{cases} \left(\frac{\mu F_n}{A_s}\right)\omega r; T < T_{melt} \\ 0 \qquad ; T \geq T_{melt} \end{cases} \tag{3}$$

The boundary condition of heat flux at the interface of the shoulder/work piece is given by the author as illustrated in equation 4. [22].

$$K\frac{\partial T}{\partial n}\Big/_{\Gamma} = q_i \tag{4}$$

The boundary condition of heat flux at the interface of the pin work piece is illustrated in equation 5. [22].

$$K\frac{\partial T}{\partial n}\Big/_{\Gamma} = q_p \tag{5}$$

The convective boundary condition of the surfaces of the work piece is exposed to the environment as shown in equation 6. [26], [22], [24].

$$K\frac{\partial T}{\partial n}\Big/_{\Gamma} = h\,(T - T_o) \tag{6}$$

### 2.1. Simulation Model

The simulation model is composed of 6061-T6 Aluminum and AZ31B Magnesium alloy plates as shown in Fig.1. The dimension of the plate for each material is 400 mm x 250 mm x 25 mm with infinite domains on both sides of the x-direction. During the FSW process, relative motion developed on the advancing and retreating sides, with the advancing side having the same direction of linear and rotational motion and the retreating side having the opposite direction of linear and rotational motion. The temperature on the advancing side is higher than on the retreating side because there is more shearing action as a positive velocity component on the advancing side, and it does not affect magnesium since its melting temperature is lower than that of aluminum [27]. The experiment was conducted using magnesium alloy on the advancing side since aluminum alloy has a higher yield strength than magnesium alloy [4].

The lower process temperature and defect-free weld zone can be obtained by placing the harder material with a higher melting temperature on the advancing side [28], [5]. As a result, in this investigation, magnesium was placed on the retreating side (RS), whereas aluminum was placed on the advancing side (AS). The plate's heat transfer with conductive and convective

terms in the welding tool and the coordinate system was fixed and shown by equation 7. [1], [25].

$$\nabla . (-\lambda \nabla T) = Q - \rho C_p W_V . \nabla T \quad (7)$$

Due to the surface-to-ambient radiation and natural convection, the aluminum and magnesium plates lose their heat on their lower and upper surfaces and the heat flux equation corresponds to those surfaces given in equations 8, 9. [1], [29], [25].

$$q_{up} = h_{up}(To - T) + \varepsilon\sigma(T_a{}^4 - T^4) \quad (8)$$

$$q_{low} = h_{low}(To - T) + \varepsilon\sigma(T_a{}^4 - T^4) \quad (9)$$

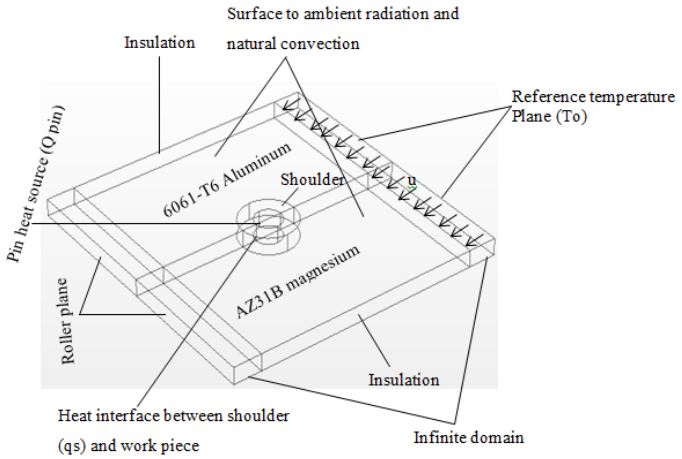


Fig. 1. Friction stir welding model geometry

The temperature is equilibrium through surface ambient radiation and natural convection with the temperature at infinity due to the infinite domain being modeled on the left side. The convective heat transfer coefficient maximum value ranges between 5 to 25 W/($m^2$·K) [28]. Therefore, the coefficient of heat transfer in this study is $h_{low}$= 6.25 W/ ($m^2$·K) and $h_{up}$ = 12.25 W/ ($m^2$·K).

Equation 10 shows the simulation's initial condition [29], [26]

$$T(x, y, z, 0) = T_i \quad (10)$$

The governing equations consist of the energy equation, continuity equation and momentum equation are given in equations 11, 12, and 13. [16].

$$\nabla . (\rho \vec{v}) + \frac{\partial \rho}{\partial t} = 0 \quad (11)$$

$$\frac{\partial(\rho \vec{v})}{\partial t} + \nabla . (\rho \vec{v} \vec{v}) = -\nabla P + \nabla . [\mu_{mix}(\nabla \vec{v} + \nabla \vec{v}^T)] \quad (12)$$

$$\frac{\partial(\rho H_{mix})}{\partial t} + \nabla . (\rho \vec{v} H) = \nabla . (\lambda \nabla T) + S_v \quad (13)$$

According to the volume of fraction model, the two alloys of materials volume fraction is given by:

$$\phi_{mix} = \alpha_{Al}\phi_{Al} + \alpha_{Mg}\phi_{Mg} \quad (14)$$

The aluminum's volume fraction is calculated as:

$$\frac{\partial(\alpha_{Al}\rho_{Al})}{\partial t} + \nabla . (\alpha_{Al}\rho_{Al}\vec{v}_{Al}) = \dot{m}_{Mg,Al} - \dot{m}_{Al,Mg} \quad (15)$$

The Magnesium's volume fraction is given by:

$$\alpha_{Mg} = 1 - \alpha_{Al} \tag{16}$$

As the work piece temperature was increased to the maximum value, the coefficient of friction is minimum and then approached zero. The coefficient of friction is about 0.2 at room temperature of the aluminum work piece [27]. Since the melting temperature of aluminum and magnesium is nearer to each other and the temperature is at ambient temperature (25°C) of the workpiece thus the friction coefficient was considered as 0.18 for this simulation experiment.

### 2.2. Meshed model

Free quadrilateral, triangular and swept (to distribute mesh in all bodies of material) are applied in the meshing of the 3D model as illustrated in Fig. 2. The meshed model obtained values of 5838 elements and 8439 mesh vertices.

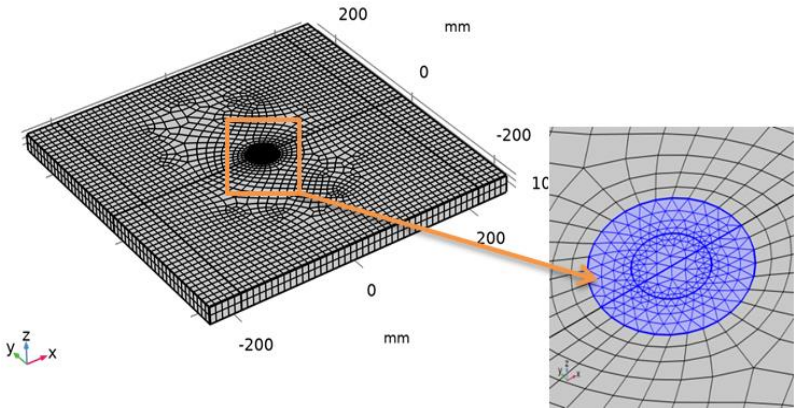


Fig. 2. Meshed model

## 3. Design of Simulation

The RSM method is used to determine the practical relationship between the response and the independent variables. Equation 17 shows the process variable function that indicates the response peak temperature ($T_P$) [30].

$$T_R = \Phi\,(R_n, W_v, S_p, F_n) + e_{ui} \tag{17}$$

When the mathematical form Φ is unknown, it is possible to accurately approximate this function within the experimental region by using polynomials stated as processing parameters variables.

The Design Expert-V13 software is utilized to design the simulation experiment while the Box-Behnken Design (BBD) of Response surface methodology (RSM) is used to create the simulation experimental design as per the procedure given by the author [31]. The author [32] reviewed the RSM methodology to measure the behaviour of the tensile strength in the friction stir welding process considering welding speed, tool rotational speed, axial load, and geometry of the tool. The experimental program consisted of four-factors and three levels which are given standard codes (-1, 0, and +1) as shown in Table. 1 [33]. The three levels (-1, 0, and +1) are also assigned for BBD methodology and Table 2 shows the 29 runs of simulation experimental sets of the actual state. The dissimilar metals of 6061-T6 Al alloys and AZ31B Mg alloys are welded using the FSW process and the input parameters are tool rotation speed, welding speed,

shoulder-to-pin diameter ratio and plunge force and output parameter as peak temperature are considered in this study and are selected based on the suggestions by (1), [10], [13], [14], [27], [29] and the factorial level ranges are selected by the guidelines given by [34]. The chemical and mechanical properties of AZ31B and 6061-T6 alloys are shown in Tables 3 and 4. The simulation experiment is conducted using COMSOL Multiphysics® 6.0 software and the output from for first run is illustrated in Fig. 3. The second-order mathematical quadratic model consists of 29 sets of experiments that estimate the process parameter's linear, quadratic, and interaction effects. The analysis of variance method is used to study both the performance characteristics of the welding operations and the interaction effect of all parameters. The Artificial Neural network heuristic methodology is coded, trained, and tested in MATLAB for the optimum cutting parameter leading to minimizing peak temperature.

Table 1. Process parameters and their levels

| Sl. No | FSW parameters | Factorial levels | | |
|---|---|---|---|---|
| | | -1 | 0 | +1 |
| 1 | Tool rotational speed (rpm) | 700 | 800 | 900 |
| 2 | Welding speed(mm/min) | 60 | 70 | 80 |
| 3 | Shoulder-to-pin diameter ratio | 2.5 | 3.0 | 3.5 |
| 4 | Plunge force(N) | 6,000 | 7,000 | 8,000 |

Table 2. Simulation values with responses

| SI. No | $R_n$ | $W_v$ | $S_p$ | $F_n$ | Output Responses | | |
|---|---|---|---|---|---|---|---|
| | | | | | $T_P$ - Simulation | $T_P$-Predicted by RSM | $T_P$-Predicted by ANN |
| | rpm | mm/ min | - | N | $T_{P(SIM)}$ (K) | $T_{P(RSM)}$ (K) | $T_{P(ANN)}$ (K) |
| 1 | 700 | 60 | 3 | 7000 | 676.3 | 676.17 | 676.06 |
| 2 | 800 | 60 | 3.5 | 7000 | 749.8 | 748.84 | 747.60 |
| 3 | 800 | 70 | 3 | 7000 | 734.22 | 734.00 | 732.99 |
| 4 | 800 | 70 | 3 | 7000 | 736.22 | 734.00 | 734.90 |
| 5 | 700 | 70 | 2.5 | 7000 | 687.99 | 688.85 | 685.05 |
| 6 | 900 | 70 | 3 | 8000 | 783.32 | 782.63 | 781.46 |
| 7 | 800 | 70 | 3 | 7000 | 735.53 | 734.00 | 733.93 |
| 8 | 800 | 70 | 3 | 7000 | 734.92 | 734.00 | 732.99 |
| 9 | 800 | 70 | 3.5 | 8000 | 755.95 | 756.03 | 755.88 |
| 10 | 700 | 70 | 3.5 | 7000 | 693.99 | 695.23 | 690.32 |
| 11 | 900 | 60 | 3 | 7000 | 779.94 | 779.04 | 777.12 |
| 12 | 800 | 80 | 3 | 6000 | 706.52 | 707.80 | 702.06 |
| 13 | 700 | 70 | 3 | 6000 | 689.32 | 689.20 | 685.22 |
| 14 | 900 | 70 | 2.5 | 7000 | 760.80 | 761.87 | 757.19 |
| 15 | 800 | 70 | 3.5 | 6000 | 740.33 | 739.15 | 737.24 |
| 16 | 900 | 80 | 3 | 7000 | 741.20 | 739.83 | 738.17 |
| 17 | 900 | 70 | 3.5 | 7000 | 769.54 | 770.99 | 765.53 |
| 18 | 900 | 70 | 3 | 6000 | 750.76 | 751.21 | 748.50 |
| 19 | 700 | 80 | 3 | 7000 | 694.51 | 693.92 | 690.94 |
| 20 | 800 | 80 | 2.5 | 7000 | 730.22 | 730.37 | 724.17 |
| 21 | 800 | 80 | 3 | 8000 | 753.76 | 754.92 | 750.52 |
| 22 | 800 | 70 | 3 | 7000 | 729.12 | 734.00 | 723.99 |
| 23 | 700 | 70 | 3 | 8000 | 697.12 | 695.86 | 694.00 |

| | | | | | | | |
|---|---|---|---|---|---|---|---|
| 24 | 800 | 60 | 3 | 8000 | 736.55 | 737.57 | 730.47 |
| 25 | 800 | 60 | 3 | 6000 | 745.47 | 746.61 | 741.42 |
| 26 | 800 | 70 | 2.5 | 6000 | 730.82 | 729.24 | 724.81 |
| 27 | 800 | 70 | 2.5 | 8000 | 750.76 | 750.44 | 745.71 |
| 28 | 800 | 60 | 2.5 | 7000 | 734.52 | 734.35 | 730.13 |
| 29 | 800 | 80 | 3.5 | 7000 | 732.01 | 731.37 | 730.70 |

Table 3. Chemical Composition of AZ31B and 6061-T6 Alloys

| Alloy | Al % | Mg % | Zn % | Mn % | Si % | Fe % | Cu % |
|---|---|---|---|---|---|---|---|
| Al 6061-T6 | Balance | 1.11 | 0.022 | 0.034 | 0.565 | 0.45 | 0.233 |
| AZ31B Mg | 2.95 | Balance | 0.912 | 0.31 | 0.006 | 0.004 | 0.002 |

Table 4. Mechanical properties of AZ31B and 6061-T6 Alloys

| Alloy | Density ($kg/m^3$) | Elastic modulus (GPa) | Yield strength (MPa) | Maximum tensile strength (MPa) | Elongation (%) |
|---|---|---|---|---|---|
| Al 6061-T6 | 2660 | 70 | 288 | 334 | 13 |
| AZ31B Mg | 1738 | 45 | 169 | 297 | 8 |

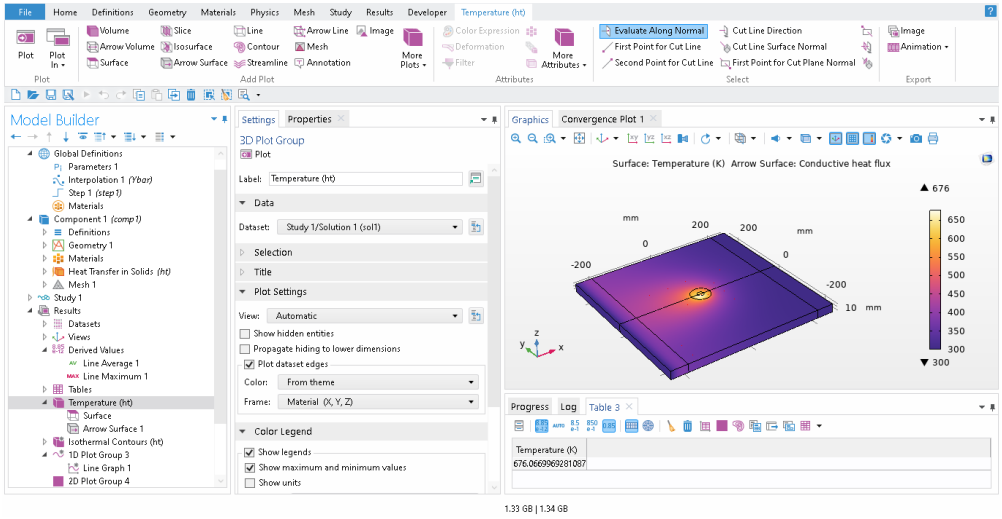


Fig. 3. COMSOL Multiphysics® 6.0 Software simulation model builder

### 3.1. Peak Temperature Prediction Using a Response Surface Model

The relationship between the y response area and the x process variable for a typical form of a quadratic polynomial is explained by the authors [35].

$$Y = \beta_0 + \beta_1 x_1 + \beta_2 x_2 + \beta_3 x_3 + \beta_{11} x_{12} + \beta_{22} x_{22} + \beta_{12} x_1 \quad (18)$$

The DESIGN EXPERT V13 software analyzes the observed simulation reading accurately. A second-order quadratic model was constructed to forecast peak temperature, and an analysis of variance was utilized to prove the model's significance. Table 5 illustrates the coefficients of determination.

Table 5. The determination coefficient

| Source | Seq. p-value | Lack of Fit (LF) p-value | Adjusted (Adj) $R^2$ | Predicted (Pred) $R^2$ | |
|---|---|---|---|---|---|
| Linear | < 0.0001 | 0.0059 | 0.8359 | 0.7804 | |
| 2FI | 0.0053 | 0.0185 | 0.9136 | 0.8194 | |
| Quadratic | < 0.0001 | 0.9580 | 0.9950 | 0.9918 | Suggested |
| Cubic | 0.9989 | 0.4372 | 0.9894 | 0.8863 | Aliased |

The coefficient of determination for determining the precision and accuracy of the model in the DOE is based on statistical analysis such as the R-squared of predictable output from input variables and the adjusted R-squared of the modified R-squared for the predictor's number in the model. Both the R-squared and adjusted R-squared determination coefficients range from 0 to 1. The values of these parameters are close to 1 or 100%, indicating a higher suggested regression model and higher model adaptation accuracy [17].

Table 6 shows the results of the ANOVA study performed to predict the peak temperature. The software suggested a quadratic model to represent the relationship between peak temperature and FSW parameters.

Table 6. ANOVA analysis of peak temperature

| Source | Sum of Squares (SS) | df | Mean Square (MS) | F-value | p-value | |
|---|---|---|---|---|---|---|
| Model | 21142.44 | 14 | 1510.17 | 395.26 | < 0.0001 | significant |
| $R_n$ -Rotational Speed | 16600.87 | 1 | 16600.87 | 4344.92 | < 0.0001 | |
| $W_v$ -Welding Speed | 345.18 | 1 | 345.18 | 90.34 | < 0.0001 | |
| $S_p$ -Shoulder-pin diameter ratio | 180.27 | 1 | 180.27 | 47.18 | < 0.0001 | |
| $F_n$ - Plunge Force | 1087.56 | 1 | 1087.56 | 284.65 | < 0.0001 | |
| $R_n W_v$ | 810.83 | 1 | 810.83 | 212.22 | < 0.0001 | |
| $R_n S_p$ | 1.88 | 1 | 1.88 | 0.4912 | 0.4949 | |
| $R_n F_n$ | 153.26 | 1 | 153.26 | 40.11 | < 0.0001 | |
| $W_v S_p$ | 45.50 | 1 | 45.50 | 11.91 | 0.0039 | |
| $W_v F_n$ | 788.49 | 1 | 788.49 | 206.37 | < 0.0001 | |
| $S_p F_n$ | 4.67 | 1 | 4.67 | 1.22 | 0.2878 | |
| $R_n^2$ | 570.88 | 1 | 570.88 | 149.42 | < 0.0001 | |
| $W_v^2$ | 36.75 | 1 | 36.75 | 9.62 | 0.0078 | |
| $S_p^2$ | 137.92 | 1 | 137.92 | 36.10 | < 0.0001 | |
| $F_n^2$ | 169.03 | 1 | 169.03 | 44.24 | < 0.0001 | |
| Residual | 53.49 | 14 | 3.82 | | | |
| Lack of Fit (LF) | 21.51 | 10 | 2.15 | 0.2691 | 0.9580 | not significant |
| Pure Error (PE) | 31.98 | 4 | 7.99 | | | |
| Cor Total (CT) | 21195.93 | 28 | | | | |

The model's F-value of 395.26 indicates that it is significant. An F-value of this size might be 0.01 percent due to noise. Significant model terms have p-values less than 0.0500. In this case, $R_n$, $W_v$, $S_p$, $F_n$, $R_nW_v$, $R_nF_n$, $W_vS_p$, $W_vF_n$, $R_n^2$, $W_v^2$, $S_p^2$ and $F_n^2$ are key model terms in this scenario.

The values above 0.1000, the model terms are insignificant. The rotating speed of the tool has a greater impact on the output.

The regression equation created by Design-Expert software V13 is revealed below.

Peak Temperature ($T_P$)

$$= +166.36900 + 2.39519R_n + 6.38140W_v - 51.53933S_p \quad 0.20327F_n - (0.01424)R_n * W_v + (0.01370)R_n * S_p + (0.00006)R_n * F_n - (0.67450)W_v * S_p + (0.00140)W_v * F_n - (0.00216)S_p * F_n - (0.00094)R_n^2 - (0.02380)W_v^2 + (18.44433)S_p^2 + (5.10483E - 06)F_n^2.$$

The F-value for Lack of Fit of 0.27 indicates that the Fit is not significant in comparison to the pure error. A significant Lack of Fit F-value owing to noise has a 95.80% chance of occurring.

## 4. Results and Discussions

Aluminum (660.3°C) and magnesium (650°C) have almost identical melting temperatures, due to this heat being equally distributed across both materials; so the joining provides an excellent outcome. The peak temperature results are predicted using RSM optimization techniques.

### 4.1. RSM Interaction Effect Analysis

#### *4.1.1. Interaction Effect of Rotational Speed vs Welding Speed Over Peak Temperature*

The interaction effect of process parameters on the peak temperature ($T_P$) is discussed below. Fig. 4(a) shows the interaction plot between rotational speed (Rn) and welding speed (Wv) with respect to peak temperature. The figure shows that the rotational speed increases consistently, and the peak temperature increases. This is owing to the fact that fewer materials were employed in the formation of the weld, which enhanced the material's flowability and lowered the forward resistance. When welding speed increases, the peak temperature decreased. As welding speed increases the frictional dissipation energy decreases thus temperature decreases The higher rotational speed causes to increase in heat energy due to friction and then a higher temperature is developed and the same report is done from the experimental investigation as reported in the [26], [27], [36].

#### *4.1.2. Interaction Effect Welding Speed vs Axial Force Over Peak Temperature*

From Fig. 4(b) it is observed as the axial force increases consistently, the peak temperature also increases but when welding speed decreases the peak temperature decreased. The plastic and friction increased as the plunge force increased and then a higher plunge force leads to penetrating material thus increasing penetration force caused to increase in maximum temperature [29], [26].

#### *4.1.3. Interaction Effect Tool Rotational Speed Vs Axial Force Over Peak Temperature*

The tool rotational speed and axial force were increased; the peak temperature is also increased as shown in Fig. 4. (c, e). This is due to the temperature being directly proportional to the rotational speed of the tool. An increase in the tool rotational speed of the tool leads to an increase in temperature. As the plunge force increased more material penetrates and then the friction dissipation energy increases thus more temperature is generated [26]. This result is supported by the experimental results of [36].

#### *4.1.4. Interaction Effect Shoulder-To-Pin Diameter Ratio Vs Welding Speed Vs Axial Force Over Peak Temperature*

As the shoulder-to-pin diameter ratio increased the peak temperature increased as shown in Fig 4. (d, f). The shoulder-to-pin diameter ratio increases the temperature of the weld zone increases due to the higher area subjected to friction that caused to higher generation of heat [1], [37]. The observed vs. predicted values with data points split by $45^o$ line as illustrated in Fig. 4(g).

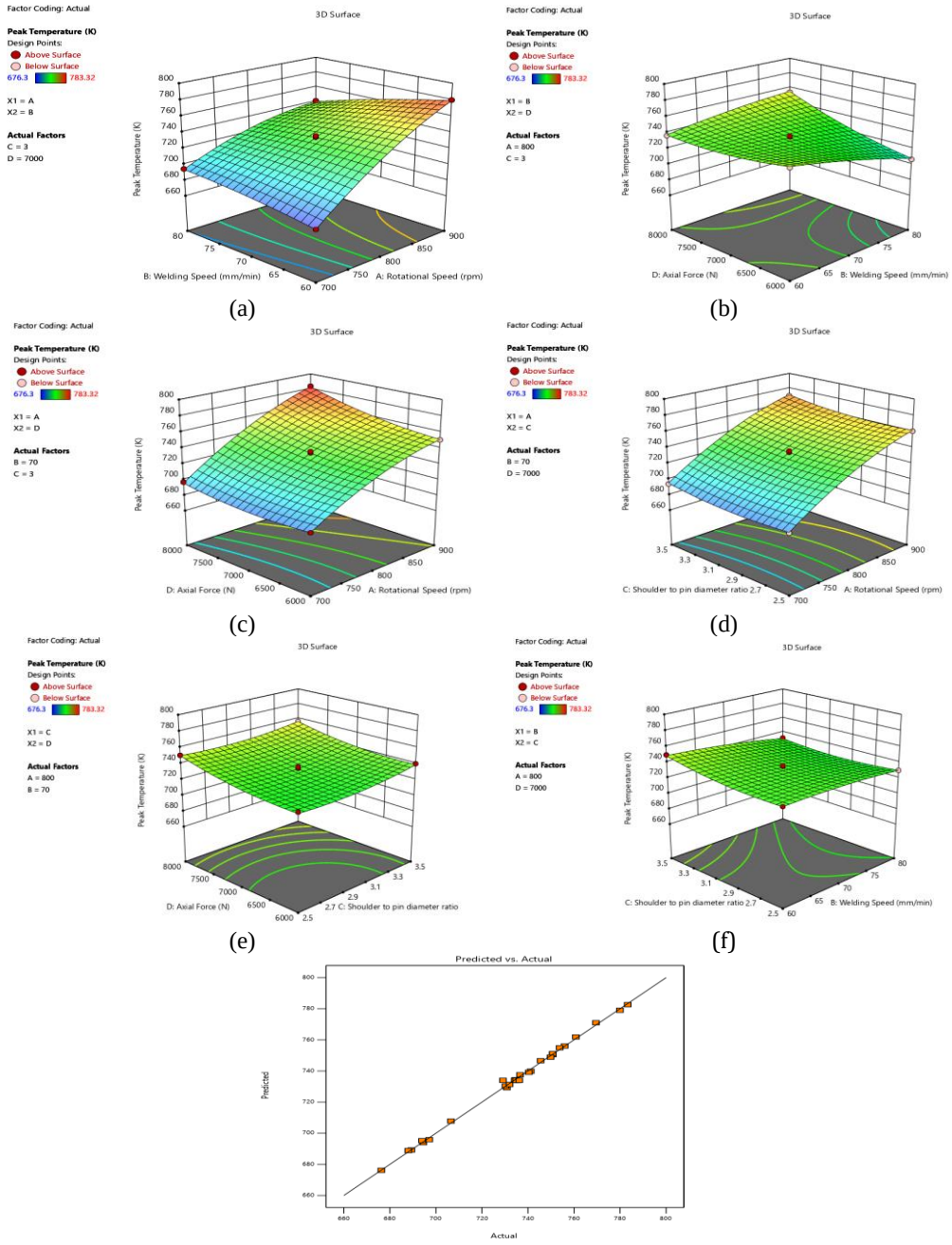


Fig. 4. 3D plot (Interaction) effect in terms of peak temperature of (a) $R_n$ vs.$W_v$, (b) $W_v$ vs. $F_n$, (c) $R_n$ vs. $F_n$, (d) $R_n$ vs. $S_p$ (e) $S_p$ vs. $F_n$, (f) $W_v$ vs. $S_p$, and (g) 2D plot of actual vs. predicted values

## 5. Artificial Neural Network

The artificial network is also called a neural network are the heart of deep learning algorithm and a subset of machine learning and used to improve the quality of mechanical research [38], [39]. The learning algorithm is being developed through ANN. Unsupervised learning and supervised learning are the two categories. The input and output in supervised are trained using the data. When operating in unsupervised mode, result data is not immediately available. Instead, additional input data, referred to as clusters, must be entered [30], [40]. It is composed of three neurons layers Input layer that consists of all input values, a hidden layer that processes hidden data and an output layer that is displayed based on input values and weight values. The outcome of the ANN architecture using MATLAB software used to predict peak temperature ($T_P$). Input, hidden, and output layers make up the network's three layers. To study the friction, stir welding parameters, the link between the input layers and the output layers is provided by the hidden layer, and the input and output layers are represented as nodes as shown in Fig. 5. The number of neurons in the input and output layers is decided based on the structure of the problem's ANN architecture level [38]. Table 7 shows the network parameter's optimal values. Four neurons are received via the input layer whereas the output has one neuron.

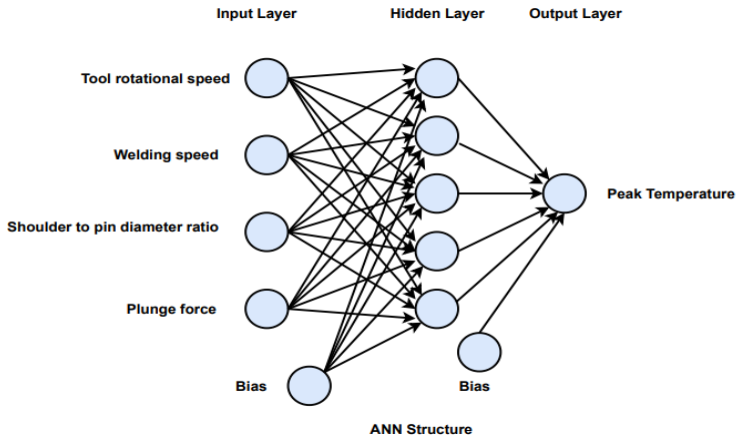


Fig. 5. ANN Structure of FSW parameters

Table 7. The ANN parameter optimum values

| SI. No | Parameter | Values |
|---|---|---|
| 1 | Input layer | 1 |
| 2 | Input layer unit | 4 |
| 3 | Hidden layer | 1 |
| 4 | Hidden layer unit | 5 |
| 5 | Output layer | 1 |
| 6 | Output layer unit | 1 |
| 7 | Epochs | 1000 |
| 8 | Algorithm | Back propagation |
| 9 | Learning rule | Gradient descent rule |

The use of Artificial Neural Networks (ANN) in welding process prediction reduces the dependable on traditional statistical methods due to their ability to excel at pattern recognition

in large datasets, thus minimizing the need for costly physical experiments while efficiently determining optimal parameter combinations and predictable welding conditions.

This study employs the neural network back propagation network technique. Input parameters include tool rotating speed, welding speed, shoulder-to-pin diameter ratio, and axial force, while output parameters include peak temperature. The prediction of peak temperature in ANN is accomplished by 1000 iterations using MATLAB software. The major procedures included developing a regression equation for performance validation of simulation data, calculating projected value, and training the algorithm.

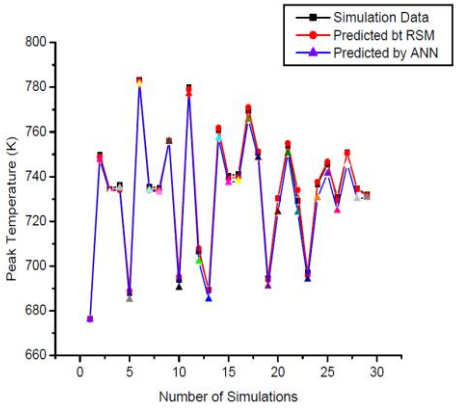


Fig.6 Comparison relationship of simulation ($T_{P(SIM)}$), RSM ($T_{P(RSM)}$) and ANN ($T_{P(ANN)}$)

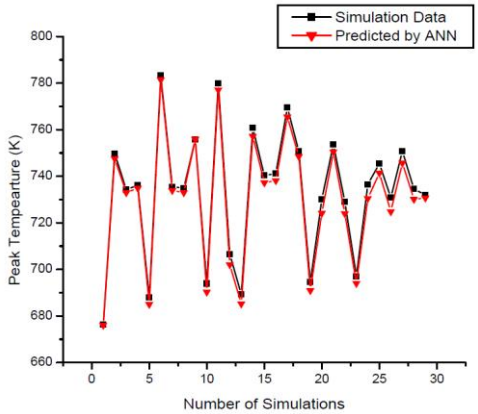


Fig.7 Comparison relationship of simulation ($T_{P(SIM)}$) and ANN ($T_{P(ANN)}$)

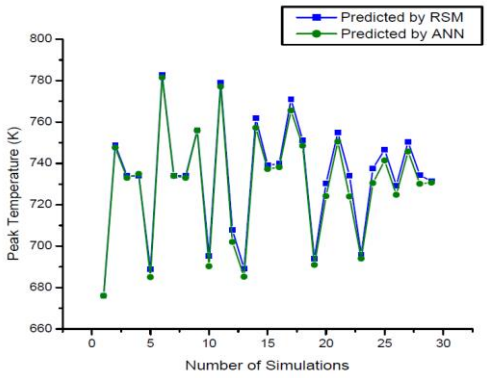


Fig. 8. Comparison of RSM ($T_{P\ (RSM))}$ and $T_{P(ANN))}$

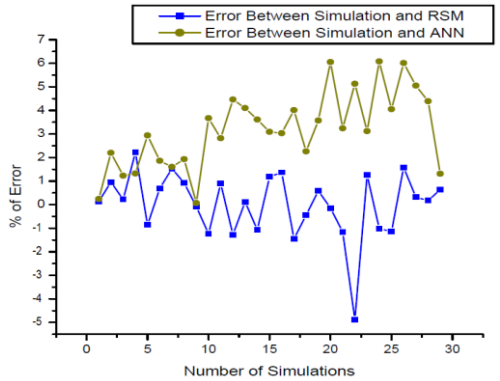


Fig.9 Error Percentage ($T_{P(RSM)}$ vs ($T_{P(ANN)}$).

Fig. 6 displays the results of the simulation, RSM, and trained ANN data. This graph demonstrates that the simulation, Design Expert software-derived RSM result, and ANN result are close to their output values. Fig. 7 displays the results of the simulation and trained ANN data. This graph demonstrates that assessments are true to their values and that experimental results achieved by utilizing ANN are quite near. Fig. 8 displays the RSM and ANN error percentages above the experimental value. The error percentage between the simulation to RSM and ANN is shown in Fig. 9. The RSM results have a higher standard deviation than the ANN projected values. It was effective in training the ANN to perform better predictions than RSM.

## 6. Validation of The Model

Table 2 shows the predicted experimental simulation result ($T_{P(RSM)}$ ) of a regression model developed using BBD by the RSM of DOE. The first 20 data sets are chosen from the 29 datasets acquired to train the ANN model; the remaining 9 data sets are chosen for testing. The ANN predicted optimum conditions were further validated with physical simulation measurements. Table 8 shows the results of the error comparison of predicted (ANN) and simulation results. An average prediction error is 0.0672017 and a maximum prediction error is 0.178959. The percentage of error is found to be within ±2 % which shows the validity of the model. The result obtained from ANN has an excellent agreement with the simulation results.

Table 8. Error Comparison of predicted (ANN) and simulation result.

| Sl. No | $R_n$ | $W_v$ | $S_p$ | $F_n$ | Output Responses | | |
|---|---|---|---|---|---|---|---|
| | | | | | Temperature - Simulation | Predicted by ANN | Error % |
| | rpm | mm/min | - | N | $T_{P\ (SIM)}$ (K) | $T_{P\ (ANN)}$ (K) | |
| 21 | 800 | 80 | 3 | 8000 | 753.76 | 753.52 | 0.03184 |
| 22 | 800 | 70 | 3 | 7000 | 729.12 | 728.99 | 0.01783 |
| 23 | 700 | 70 | 3 | 8000 | 697.12 | 696.00 | 0.160661 |
| 24 | 800 | 60 | 3 | 8000 | 736.55 | 736.47 | 0.010861 |
| 25 | 800 | 60 | 3 | 6000 | 745.47 | 745.42 | 0.006707 |
| 26 | 800 | 70 | 2.5 | 6000 | 730.82 | 729.81 | 0.138201 |
| 27 | 800 | 70 | 2.5 | 8000 | 750.76 | 750.71 | 0.00666 |
| 28 | 800 | 60 | 2.5 | 7000 | 734.52 | 734.13 | 0.053096 |
| 29 | 800 | 80 | 3.5 | 7000 | 732.01 | 730.70 | 0.178959 |
| % of error | | | | | | | 0.0672017 |

## 7. Conclusion

The Design Expert-V13 software package is employed to design BBD and used to create a second-order mathematical model to predict peak temperature in friction stir welding of dissimilar alloy metals AZ31B Mg and 6061-T6 Al with varying tool rotational speed, welding speed, shoulder-to-pin diameter ratio, and plunge force as input parameters. The simulation is carried out using the COMSOL Multiphysics® 6.0 Software. The two-stage attempt has been carried out to forecast peak temperature using surface response methodology and optimization is done using artificial neural networks. The results are fairly useful to achieve predictable process parameters and predictable peak temperature.

- The model generated by RSM is capable of providing accurate projected peak temperature values that are similar to the actual values obtained in the simulation experiments. The ANOVA was used to check the adequacy levels with a confidence level of 95 %.
- The direct and interaction impacts were discussed, and it is revealed that rotational speed has the greatest effect as compared to other parameters. From the result, the rotating speed rises, the temperature also increases. It is clear from this study that the best minimum peak temperature ($T_P$) values attained at Tool rotational speed ($R_n$) of 700 rpm, welding speed ($W_v$) of 60 mm/min, shoulder-to-pin diameter ratio ($S_p$) of 3 and plunge force ($F_n$) of 7000 N.
- Finally, the peak temperature was optimized using an Artificial Neural Network (ANN). The ANN predicts minimal peak temperature and the percentage of error is

less than 2% error percentage. The confirmatory test shows that the ANN and simulation results are extremely close to each other.

**Acknowledgment**

The research was supported by the INDMET project (Grant No.62862) funded by the NORHED II programme.

**Abbreviations**

| SI. No | Name | Description | Units |
|---|---|---|---|
| 1 | $\alpha_{Al}$ | Volume fraction of Al alloy in the mixture | - |
| 2 | $\alpha_{Mg}$ | Volume fraction of Mg alloy in the mixture | - |
| 3 | $A_s$ | Shoulder's surface area | $m^2$ |
| 4 | $\beta_0$ | constant | - |
| 5 | $\beta_1$, $\beta_2$, $\beta_3$ | linear term coefficient | - |
| 6 | $\beta_{11}$, $\beta_{22}$ | quadratic term coefficient | - |
| 7 | $\beta_{12}$ | interaction term coefficient | - |
| 8 | $C_p$ | Specific heat capacity | J/kg. K |
| 9 | $\varepsilon$ | Surface emissivity | $W/m^2$ |
| 10 | $e_u$ | Residual | - |
| 11 | $F_n$ | Plunge force | N |
| 12 | $F_p$ | Translation force | N |
| 13 | $\nabla$ | Gradient operator | - |
| 14 | $\partial T/\partial n$ | Temperature gradient normal to the boundary | K/m |
| 15 | h | Coefficient of convection | $W/m^2$. K |
| 16 | $H_{mix}$: | Enthalpy of the material mixture | J/kg |
| 17 | $h_{up}$, $h_{low}$ | Upper and lower surface convective heat transfer coefficient | $W/m^2$.K |
| 18 | $i_u$ | Reflects the level of the $i^{th}$ factor in the $u^{th}$ observation | - |
| 19 | $\lambda$ | Thermal conductivity | W/m.K |
| 20 | $\lambda_x$, $\lambda_y$, $\lambda_z$ | Thermal conductivity in x, y and z direction | W/m.K |
| 21 | $\mu$ | Coefficient of friction | - |
| 22 | $\lambda_T$ | Thread's helix angle | rad |
| 23 | $\mu_{mix}$ | Viscosity of the mixture property of the material | N.s/$m^2$ |
| 24 | $\dot{m}_{Al,Mg}$ | Mass flow rate of aluminum into magnesium | kg/s |
| 25 | $\dot{m}_{Mg,Al}$ | Mass flow rate of magnesium into aluminum | kg/s |
| 26 | n | Direction vector normal for boundary $\Gamma$ | - |
| 27 | P | Pressure | Pa |
| 28 | $\rho$ | Density | kg/$m^3$ |
| 29 | $\rho_{Al}$ | Density of Al alloy | kg/$m^3$ |
| 30 | $\phi$Al and $\phi$Mg | Material properties of Al and Mg alloys | - |
| 31 | $\phi_{mix}$ | Mixture material property | - |
| 32 | $q_p$ | Heat generated at tool pin/work piece interface | J |
| 33 | $q_i$ | Heat generated at tool shoulder/work piece interface | J |
| 34 | $q_s$ | Shoulder's heat flux | $W/m^2$ |
| 35 | $\Phi$ | Response surface | - |
| 36 | $R_n$ | Tool rotational speed | m/s |
| 37 | $r_p$ | Pin radius | mm |
| 38 | $\tau$ | Material's shear stress | MPa |
| 39 | $S_p$ | Shoulder-to-pin diameter ratio | - |
| 40 | $S_v$ | Volumetric heat source | J/$m^3$ |
| 41 | $\sigma$ | Stefan-Boltzmann constant | $W/m^2.K^4$ |

| | | | |
|---|---|---|---|
| 42 | T | Temperature | K |
| 43 | $T_a$ | Ambient temperature | K |
| 44 | $T_o$ | Reference temperature | K |
| 45 | $T_P$ | Peak Temperature | K |
| 46 | $T_R$ | Temperature rise | K |
| 47 | T (x, y, z, 0) | Temperature (K) at Coordinates (x, y, z) when t = 0 | K |
| 48 | $t_w$ | Work piece thickness | mm |
| 49 | u | Number of observations in the factorial experiment | - |
| 50 | $\vec{v}$ | Velocity vector | m/s |
| 51 | $\vec{v}Al$ | Velocity vector of Aluminium | m/s |
| 52 | $W_v$ | Welding speed | m/s |
| 53 | ω | Tool's angular velocity | rad/s |

## References


[1] Vignesh RV, Padmanaban R, Arivarasu M, Thirumalini S, Gokulachandran J, Ram MSSS. Numerical modelling of thermal phenomenon in friction stir welding of aluminum plates. IOP Conf Ser Mater Sci Eng. 2016;149(1). https://doi.org/10.1088/1757-899X/149/1/012208

[2] Somasekharan AC, Murr LE. Fundamental studies of the friction-stir welding of magnesium alloys to 6061-T6 Aluminum. Magnes Technol. 2004;3:31-6.

[3] Woo W, Choo H. Softening behaviour of friction stir welded Al 6061-T6 and Mg AZ31B alloys. Sci Technol Weld Join. 2011;16(3):267-72. https://doi.org/10.1179/1362171811Y.0000000016

[4] Dorbane A, Mansoor B, Ayoub G, Shunmugasamy VC, Imad A. Mechanical, microstructural and fracture properties of dissimilar welds produced by friction stir welding of AZ31B and Al6061. Mater Sci Eng A [Internet]. 2016;651:720-33. https://doi.org/10.1016/j.msea.2015.11.019

[5] Mansoor B, Dorbane A, Ayoub G, Imad A. Friction stir welding of AZ31B magnesium alloy with 6061-T6 Aluminum alloy: Influence of processing parameters on microstructure and mechanical properties. Frict Stir Weld Process VIII. 2016;259-66. https://doi.org/10.1007/978-3-319-48173-9_28

[6] Wu B, Liu J, Song Q, Lv Z, Bai W. Controllability of joint integrity and mechanical properties of friction stir welded 6061-T6 Aluminum and AZ31B magnesium alloys based on stationary shoulder. High Temp Mater Process. 2019;38(2019):557-66. https://doi.org/10.1515/htmp-2019-0001

[7] Zheng Y, Pan X, Ma Y, Liu S, Zang L, Chen Y. Microstructure and corrosion behavior of friction stir-welded 6061 Al/AZ31 Mg joints with a Zr interlayer. Materials (Basel). 2019;12(7). https://doi.org/10.3390/ma12071115

[8] Liu H, Chen Y, Yao Z LF. Effect of Tool Offset on the Microstructure and Properties of AA6061/AZ31B Friction Stir Welding Joints. Metals (Basel). 2020;10:1-9. https://doi.org/10.3390/met10040546

[9] Kumar U, Prajapati A, Acharya U, Medhi T, Saha Roy B, Saha SC. Welding condition & microstructure of friction stir welded AA 6061-T6 and AZ31B. Mater Today Proc [Internet]. 2019;46:9484-9. https://doi.org/10.1016/j.matpr.2020.03.242

[10] Saldaña-Garcés R, Hernández-García D, García-Vázquez F, Gutiérrez-Castañeda EJ, Verdera D, Deaquino-Lara R. Friction stir welding of dissimilar aa6061-t6 to az31b-h24 alloys. Soldag e Insp. 2020;25:1-14. https://doi.org/10.1590/0104-9224/si25.25

[11] Xu Y, Ke L, Ouyang S, Mao Y, Niu P. Precipitation behavior of intermetallic compounds and their effect on mechanical properties of thick plate friction stir welded Al/Mg joint. J Manuf Process [Internet]. 2021;64(December 2020):1059-69. https://doi.org/10.1016/j.jmapro.2020.12.068

[12] Rajesh Jesudoss Hynes N, Vivek Prabhu M, Shenbaga Velu P, Kumar R, Tharmaraj R, Farooq MU, et al. An experimental insight of friction stir welding of dissimilar AA 6061/Mg AZ 31 B joints. Proc Inst Mech Eng Part B J Eng Manuf. 2022;236(6-7):787-97. https://doi.org/10.1177/09544054211043474
[13] Mughal MP, Nawaz A, Raza SF. Friction Stir Welding of Magnesium AZ31B and Aluminum Al-6062. Adv Transdiscipl Eng. 2022;25:135-42. https://doi.org/10.3233/ATDE220580
[14] Sarila V, Koneru HP, Cheepu M, Chigilipalli BK, Kantumuchu VC, Shanmugam M. Microstructural and Mechanical Properties of AZ31B to AA6061 Dissimilar Joints Fabricated by Refill Friction Stir Spot Welding. J Manuf Mater Process. 2022;6(5). https://doi.org/10.3390/jmmp6050095
[15] Huang T, Zhang Z, Liu J, Chen S, Xie Y, Meng X, et al. Interface Formation of Medium-Thick AA6061 Al/AZ31B Mg Dissimilar Submerged Friction Stir Welding Joints. Materials (Basel). 2022;15(16). https://doi.org/10.3390/ma15165520
[16] Yang C, Shi Q, Chen G. A Simulation Study on Material Flow and Mixing Mechanism in Dissimilar Friction Stir Welding of AA6061 and AZ31 Alloys [Internet]. Springer Nature Switzerland; 2023. 227-236. https://doi.org/10.1007/978-3-031-22661-8_21
[17] Ghiasvand A, Suksatan W, Tomków J, Rogalski G, Derazkola HA. Investigation of the Effects of Tool Positioning Factors on Peak Temperature in Dissimilar Friction Stir Welding of AA6061-T6 and AA7075-T6 Aluminum Alloys. Materials (Basel). 2022;15(3). https://doi.org/10.3390/ma15030702
[18] Khalaf HI, Al-Sabur R, Demiral M, Tomków J, Łabanowski J, Abdullah ME, Aghajani Derazkola H. The Effects of Pin Profile on HDPE Thermomechanical Phenomena during FSW. Polymers. 2022; 14(21): 4632. https://doi.org/10.3390/polym14214632
[19] Al-Sabur R, Khalaf HI, Świerczyńska A, Rogalski G, Derazkola HA. Effects of noncontact shoulder tool velocities on friction stir joining of polyamide 6 (PA6). Materials. 2022; 15(12): 4214. https://doi.org/10.3390/ma15124214
[20] Sidhu RS, Kumar R, Kumar R, Goel P, Singh S, Pimenov DY, Giasin K, Adamczuk K. Joining of Dissimilar Al and Mg Metal Alloys by Friction Stir Welding. Materials. 2022; 15(17): 5901. https://doi.org/10.3390/ma15175901
[21] Khalaf HI, Al-Sabur R, Derazkola, HA. Effect of number of tool shoulders on the quality of steel to magnesium alloy dissimilar friction stir welds. Archives of Civil and Mechanical Engineering. 2023; 23(2):125. https://doi.org/10.1007/s43452-023-00673-z
[22] Song M, Kovacevic R. Thermal modeling of friction stir welding in a moving coordinate system and its validation. Int J Mach Tools Manuf. 2003;43(6):605-15. https://doi.org/10.1016/S0890-6955(03)00022-1
[23] Chikh A, Serier, Al-Sabur R, Siddiquee AN, Gangil N. Thermal modeling of tool-work interface during friction stir welding process. Russian Journal of Non-Ferrous Metals. 2022; 63(6): 690-700. https://doi.org/10.3103/S1067821222060049
[24] Colegrove P. 3 Dimensional Flow and Thermal Modelling of the Friction Stir Welding Process. 2nd Int Symp Frict Stir Weld. 2000;(January):1-11.
[25] Tayo OA, Laseinde TO, Mashinini M. Finite-element modeling of thermo-mechanical phenomena in friction stir welding of AISI 4340 steel. Proc Int Conf Ind Eng Oper Manag. 2019;1215-21.
[26] Aziz SB, Dewan MW, Huggett DJ, Wahab MA, Okeil AM, Liao TW. Impact of Friction Stir Welding (FSW) process parameters on thermal modeling and heat generation of aluminum alloy joints. Acta Metall Sin (English Lett. 2016;29(9):869-83. https://doi.org/10.1007/s40195-016-0466-2
[27] Meyghani B, Awang M. Developing a Finite Element Model for Thermal Analysis of Friction Stir Welding (FSW) Using Hyperworks. Lect Notes Mech Eng. 2020;619-28. https://doi.org/10.1007/978-981-13-8297-0_64
[28] Al-Badour F, Merah N, Shuaib A, Bazoune A. Thermo-mechanical finite element model of friction stir welding of dissimilar alloys. Int J Adv Manuf Technol. 2014;72(5-8):607-17. https://doi.org/10.1007/s00170-014-5680-3

[29] Lemi MT, Gutema EM, Gopal M. Modeling and simulation of friction stir welding process for AA6061-T6 aluminum alloy using finite element method. Eng Solid Mech. 2022;10(2):139-52. https://doi.org/10.5267/j.esm.2022.2.001
[30] Gopal M. Prediction of surface roughness in turning of duplex stainless steel (DSS) using response surface methodology (RSM) and artificial neural network (ANN). Mater Today Proc [Internet]. 2020;47:6704-11. https://doi.org/10.1016/j.matpr.2021.05.118
[31] Harachai K, Prasomthong, S. Investigation of the optimal parameters for butt joints in a friction stir welding (FSW) process with dissimilar aluminum alloys. Materials Research Express, 2023, 10(2), p.026514. https://doi.org/10.1088/2053-1591/acbb54
[32] Al-Sabur R. Tensile strength prediction of aluminum alloys welded by FSW using response surface methodology-Comparative review. Materials Today: Proceedings, 2021 45, pp.4504-4510. https://doi.org/10.1016/j.matpr.2020.12.1001
[33] Box GE DN. Empirical model-building and response surfaces. John Wiley & Sons; 1987.
[34] Hoyos E, Serna, MC. Basic tool design guidelines for friction stir welding of aluminum alloys. Metals. 2021; 11(12), p.2042. https://doi.org/10.3390/met11122042
[35] Gutema EM, Gopal M, Lemu HG. Temperature Optimization by Using Response Surface Methodology and Desirability Analysis of Aluminum 6061. Materials (Basel). 2022;15(17). https://doi.org/10.3390/ma15175892
[36] Tang W, Guo X, McClure JC, Murr LE, Nunes A. Heat input and temperature distribution in friction stir welding. J Mater Process Manuf Sci. 1998;7(2):163-72. https://doi.org/10.1106/55TF-PF2G-JBH2-1Q2B
[37] Akbari M, Aliha MRM, Keshavarz SME, Bonyadi A. Effect of tool parameters on mechanical properties, temperature, and force generation during FSW. Proc Inst Mech Eng Part L J Mater Des Appl. 2019;233(6):1033-43. https://doi.org/10.1177/1464420716681591
[38] Uday KN, Rajamurugan G. Analysis of tensile strength on friction stir welded Al 6061 composite reinforced with B4C and Cr2O3 using RSM and ANN. Eng Res Express. 2023;5(1):0-15. https://doi.org/10.1088/2631-8695/acb6d1
[39] Mahajan L, Bhagat S. An artificial neural network for the prediction of the strength of supplementary cementitious concrete. Res Eng Struct Mater. 2022;8(2):421-30. https://doi.org/10.17515/resm2022.341st0918tn
[40] Asiltürk I, Çunkaş M. Modeling and prediction of surface roughness in turning operations using artificial neural network and multiple regression method. Expert Syst Appl. 2011;38(5):5826-32. https://doi.org/10.1016/j.eswa.2010.11.041